Multigrid Acceleration of the Flux-Split Euler Equations

W. Kyle Anderson* and James L. Thomas*
NASA Langley Research Center, Hampton, Virginia
and
David L. Whitfield†
Mississippi State University, Mississippi State, Mississippi

Multigrid acceleration is applied to a flux-split algorithm for solving the Euler equations in three dimensions. The basic algorithm is an implicit spatially split approximate factorization method. The stability and performance of the scheme in comparison to other factorizations are examined. Results are presented for three-dimensional flows that demonstrate substantially improved convergence with the multigrid algorithm.

Introduction

UPWIND difference schemes for solving the Euler equations are becoming increasingly popular for several reasons. The time-dependent Euler equations form a system of hyperbolic equations and upwind differencing models the characteristic nature of the equations in that information at each grid point is obtained from directions dictated by characteristic theory. The resulting methods can capture strong shocks without any oscillations. Explicitly applied artificial viscosity is not required for stability, and hence arbitrary smoothing constants are eliminated.

The particular upwind method used here is the flux-vector splitting method in which the flux vectors are split into forward and backward contributions based on an eigenvalue decomposition and differenced accordingly. The splittings investigated to date are those of Steger and Warming,[1] Steger,[2] and Buning and Steger[3] and Van Leer[4] and Anderson et al.[5] Recently, these two splittings were compared using an implicit scheme and it was shown that the Van Leer splitting yielded sharper shocks (generally only one transition point) and was more robust than the Steger-Warming splitting; it is, therefore, used exclusively in the present study. The advantages of flux splitting are obtained at the cost of increased computational work in comparison to unsplit methods, since two sets of fluxes are computed for each coordinate direction, and implicit schemes require two sets of flux Jacobians (e.g., $\partial F^+/\partial Q$ and $\partial F^-/\partial Q$) for consistent linearization of the fluxes. In addition, the split fluxes and flux Jacobians are also generally more complicated than the unsplit terms owing to the branching involved with eigenvalue sign changes. In order to offset the additional expense of the upwind methods, it is highly desirable to accelerate the convergence rate, especially when only steady-state solutions are sought; the objective is to reduce the computer time required while still maintaining the high level of robustness and accuracy attained from upwind differencing. Accelerating the convergence rate becomes increasingly important as the mesh is refined since the convergence rate for single-grid methods deteriorates with increasing mesh size, making computations on very fine meshes prohibitively expensive.

One method that has been successful in accelerating the convergence rate of elliptic problems, attaining a spectral radius independent of the mesh spacing, is the multigrid method.[6] Although most of the existing theory on multigrid methods pertains specifically to elliptic equations, it has been shown in several references[7-9] that the multigrid method can greatly accelerate the convergence rate of numerical schemes used for solving the Euler equations. The purpose of the current investigation is to combine the full approximation multigrid method previously implemented by Jameson and Baker[7] and Jameson and Yoon[8] with the flux-vector splitting method of Ref. 5 to obtain efficient solutions to the Euler equations in three dimensions. The baseline algorithm and the multigrid acceleration technique are described below. Results for subsonic and transonic flow over wings are given, including the influence of the mesh size on the spectral radius.

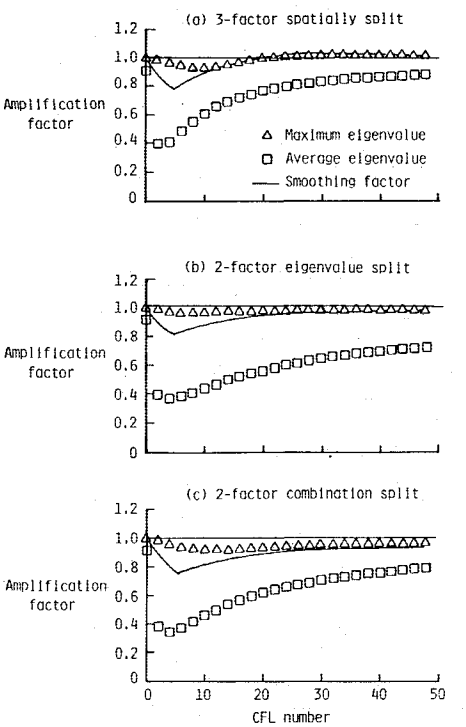

Fig. 1 Stability analysis of three-dimensional approximate factorization schemes, $M_\infty = 0.8$, $\alpha = 0$ deg.

Received Feb. 2, 1986; revision received Nov. 12, 1987.

*Research Scientist, Analytical Methods Branch, Low-Speed Aerodynamics Division. Member AIAA.
†Professor, Aerospace Engineering Department. Member AIAA.

Governing Equations

The governing equations are the time-dependent equations of ideal gas dynamics, i.e., the Euler equations, which express the conservation of mass, momentum, and energy for an inviscid nonconducting gas in the absence of external forces. The conservation form of the equations in generalized coordinates reads

$$\frac{\partial \hat{Q}}{\partial t}+\frac{\partial \hat{F}}{\partial \xi}+\frac{\partial \hat{G}}{\partial \eta}+\frac{\partial \hat{H}}{\partial \zeta}=0 \tag{1}$$

where

$$\hat{Q}=\frac{Q}{J}=\frac{1}{J}\begin{Bmatrix}\rho\\ \rho u\\ \rho v\\ \rho w\\ e\end{Bmatrix} \tag{2}$$

$$\hat{F}=\frac{1}{J}\begin{Bmatrix}\rho U\\ \rho Uu+\xi_x p\\ \rho Uv+\xi_y p\\ \rho Uw+\xi_z p\\ (e+p)U\end{Bmatrix} \tag{3}$$

$$\hat{G}=\frac{1}{J}\begin{Bmatrix}\rho V\\ \rho Vu+n_x p\\ \rho Vv+n_y p\\ \rho Vw+n_z p\\ (e+p)V\end{Bmatrix} \tag{4}$$

$$\hat{H}=\frac{1}{J}\begin{Bmatrix}\rho W\\ \rho Wu+\zeta_x p\\ \rho Wv+\zeta_y p\\ \rho Ww+\zeta_z p\\ (e+p)W\end{Bmatrix} \tag{5}$$

The equations are nondimensionalized in terms of reference density ρ_∞ and speed of sound a_∞. The Cartesian velocity components are u, v, w in the x, y, and z Cartesian directions. The pressure p is related to the conserved variables Q through the ideal gas law

$$p=(\gamma-1)[e-\rho(u^2+v^2+w^2)/2] \tag{6}$$

where γ is the ratio of specific heats, taken as $\gamma=1.4$. The equations have been generalized from Cartesian coordinates using a steady transformation of the type

$$\xi=\xi(x,y,z) \qquad \eta=\eta(x,y,z) \qquad \zeta=\zeta(x,y,z) \tag{7}$$

where the Jacobian of the transformation is denoted by J and the contravariant velocity components are

$$U=\xi_x u+\xi_y v+\xi_z w \tag{8a}$$

$$V=\eta_x u+\eta_y v+\eta_z w \tag{8b}$$

$$W=\zeta_x u+\zeta_y v+\zeta_z w \tag{8c}$$

The equations, although written in generalized coordinates, are used in a finite-volume formulation. Equation (1) can be interpreted as describing the balance of mass, momentum, and energy over an arbitrary control volume. In this connection the vectors $\text{grad}(\xi)/J$, $\text{grad}(\eta)/J$, and $\text{grad}(\zeta)/J$ represent directed areas of cell interfaces in the ξ, η, and ζ directions, and the Jacobian J represents the inverse of the cell volume. Likewise, the quantities $\rho U/J$, $\rho V/J$, and $\rho W/J$ represent the mass flux crossing the cell interfaces in the ξ, η, and ζ directions.

Flux Splitting

The upwind differencing in the present work is effected through the technique of flux-vector splitting. The generalized fluxes $\hat{F}$, $\hat{G}$, and $\hat{H}$ are split into forward and backward contributions according to the signs of the eigenvalues of the Jacobian matrices $\partial\hat{F}/\partial Q$, $\partial\hat{G}/\partial Q$, and $\partial\hat{H}/\partial Q$, and differenced accordingly. For example, considering the flux in the ξ direction

$$\delta_\xi \hat{F}=\delta_\xi^- \hat{F}^+ + \delta_\xi^+ \hat{F}^- \tag{9}$$

where δ_ξ^- and δ_ξ^+ denotes general backward and forward divided-difference operators, respectively, in the ξ direction. In this study, the particular splitting used is that developed by Van Leer.[4] It has the advantage that the individual split-flux contributions transition smoothly across eigenvalue sign changes, such as occur at sonic and stagnation points. In addition, the splitting allows normal shocks to be captured with at most two transition zones; in practice, shocks are most often captured with one transition zone, as demonstrated recently[5] for a series of airfoil flows.

The three-dimensional splitting of Van Leer in generalized coordinates is given below. Only the splitting for the flux in the ξ direction is given, as the others can be obtained similarly. The flux $\hat{F}$ is split according to the contravariant Mach number in the ξ direction, defined as $M_\xi=\bar{u}/a$, where $\bar{u}=U/|\text{grad}(\xi)|$. For supersonic flow, $|M_\xi|\geqq 1$

$$\hat{F}^+=\hat{F}, \qquad \hat{F}^-=0, \qquad M_\xi \geqq +1 \tag{10a}$$

$$\hat{F}^-=\hat{F}, \qquad \hat{F}^+=0, \qquad M_\xi \leqq -1 \tag{10b}$$

and for subsonic flow, $|M_\xi|<1$

$$\hat{F}^\pm=\frac{|\text{grad}(\xi)|}{J}\begin{Bmatrix}f^\pm_{\text{mass}}\\ f^\pm_{\text{mass}}[\hat{k}_x(-\bar{u}\pm 2a)/\gamma+u]\\ f^\pm_{\text{mass}}[\hat{k}_y(-\bar{u}\pm 2a)/\gamma+v]\\ f^\pm_{\text{mass}}[\hat{k}_z(-\bar{u}+2a)/\gamma+w]\\ f^\pm_{\text{energy}}\end{Bmatrix} \tag{11a}$$

where

$$f^\pm_{\text{mass}}=\pm\rho a(M_\xi\pm 1)^2/4 \tag{11b}$$

$$f^\pm_{\text{energy}}=f^\pm_{\text{mass}}\{[-(\gamma-1)\bar{u}^{-2}\pm 2(\gamma-1)\bar{u}a+2a^2]/(\gamma^2-1) +(u^2+v^2+w^2)/2\} \tag{11c}$$

and the direction cosines of the directed interface in the ξ direction are

$$\hat{k}_x=\xi_x/|\text{grad}(\xi)| \tag{12a}$$

$$\hat{k}_y=\xi_y/|\text{grad}(\xi)| \tag{12b}$$

$$\hat{k}_z=\xi_z/|\text{grad}(\xi)| \tag{12c}$$

The split-flux differences are implemented as a flux balance across a cell, corresponding to MUSCL-type differencing, i.e.,

$$\delta_\xi^- \hat{F}^+ + \delta_\xi^+ \hat{F}^- = [\hat{F}^+(Q^-)+\hat{F}^-(Q^+)]_{i+1/2} - [\hat{F}^+(Q^-)+\hat{F}^-(Q^+)]_{i-1/2} \tag{13}$$

The notation $\hat{F}^+(Q^-)_{i+1/2}$ denotes the forward flux evaluated using the metric terms at the cell interface $i+1/2$, and the conserved state variables on the upwind side of the interface, obtained by a fully upwind second-order state variable interpolation:

$$Q^-_{i+1/2} = 1.5\,Q_i - 0.5\,Q_{i-1} \tag{14a}$$

$$Q^+_{i+1/2} = 1.5\,Q_{i+1} - 0.5\,Q_{i+2} \tag{14b}$$

Here, $Q^n_{i,j,k}$ denotes the average value of Q in the cell centered on (ξ_i, η_j, ζ_k) at time t^n; for simplicity, wherever the script notation is i, j, k, or n, it is most often dropped.

Baseline Algorithm

The baseline single-grid algorithm is a backward Euler time integration scheme that uses approximate factorization to split the resulting large-banded block matrix equation into a sequence of easily invertible equations.[10] When using flux-vector splitting, there are numerous ways of factoring the implicit operator into a sequence of simpler operators.[1] For many of the results shown below, the scheme chosen is a spatially split algorithm given in three dimensions by

$$[I + \Delta t(\delta_\xi^- A^+ + \delta_\xi^+ A^-)][I + \Delta t(\delta_\eta^- B^+ + \delta_\eta^+ B^-)]$$
$$[I + \Delta t(\delta_\zeta^- C^+ + \delta_\zeta^+ C^-)]\Delta Q = -\Delta t R^n \tag{15}$$

The scheme requires the solution to a system of block tridiagonals for each factor, but has the advantage of being completely vectorizable, and viscous effects can be easily incorporated. The block tridiagonal matrices can be solved with vector lengths corresponding to the number of lines in the grid. The three-dimensional computations in the present implementation take advantage of the large memory available on the VPS-32 computer at NASA Langley, and solve the block matrix equations over multiple planes simultaneously, yielding longer vector lengths and faster processing rates.

At least two other ways to factor the implicit operator in three dimensions are possible and have been recently utilized.[11] The first is a two-factor method in which the implicit operator is factored such that one operator contains the Jacobians with all positive eigenvalues, and the other operator contains the Jacobians with all negative eigenvalues. The scheme can be written as

$$[I + \Delta t(\delta_\xi^- A^+ + \delta_\eta^- B^+ + \delta_\zeta^- C^+)]$$
$$[I + \Delta t(\delta_\xi^+ A^- + \delta_\eta^+ B^- + \delta_\zeta^+ C^-)]\Delta Q = -\Delta t R^n \tag{16}$$

The scheme has low-factorization error and only requires the solution of block bidiagonal equations. In the present implementation, most of the algorithm is vectorizable; the only scalar computations correspond to back substitutions along a line. It should be noted, however, that this algorithm can be completely vectorized along diagonal planes.

The last scheme considered is another two-factor scheme that is spatially split in two directions, with the third direction split according to the sign of its eigenvalues. The resulting scheme, which is referred to here as combination splitting, is given by

$$[I + \Delta t(\delta_\xi^- \hat{A}^+ + \delta_\xi^+ \hat{A}^- + \delta_\zeta^- \hat{C}^+)]$$
$$[I + \Delta t(\delta_\eta^- \hat{B}^+ + \delta_\eta^+ \hat{B}^- + \delta_\zeta^+ \hat{C}^-)]\Delta\hat{Q} = -\Delta t R^n \tag{17}$$

This scheme also requires the solution of block tridiagonal systems and is completely vectorizable; however, the solution of each plane requires that the solution of the previous plane be known, thereby eliminating the possibility of extending the vector operations over several planes. The result is that even though this scheme requires only two-thirds of the operations of the three-factor scheme, the computational rate on the VPS-32 is actually degraded by about 10%. This, however, is likely to change on a computer whose speed is not as dependent on long vector lengths.

Stability Analysis

In order to examine the stability characteristics of the three-dimensional approximate-factorization algorithms considered above, a Fourier analysis is conducted on the complete system of equations. Because of the mixed signs of the eigenvalues of the Euler equations, and because the three-dimensional Euler equations cannot be diagonalized to yield a system of convection equations, stability analysis of the scalar convection equation is not sufficient to determine stability properties of the three schemes. The complete system of equations can be written as

$$M\Delta Q = -L = -\Delta t R^n \tag{18}$$

where for Cartesian coordinates

$$R^n = \delta_x^- F^+ + \delta_x^+ F^- + \delta_y^- G^+ + \delta_y^+ G^- + \delta_z^- H^+ + \delta_z^+ H^- \tag{19}$$

and M is an implicit operator corresponding to the scheme considered. Linearizing the residual R^n as

$$R^n = A^+\delta_x^- Q^n + A^-\delta_x^+ Q^n + B^+\delta_y^- Q^n$$
$$+ B^-\delta_y^+ Q^n + C^+\delta_z^- Q^n + C^-\delta_z^+ Q^n \tag{20}$$

and assuming that the Jacobians are locally constant, the stability can be analyzed by letting

$$Q^n = \lambda^n U_o e^{i\beta x} e^{i\gamma y} e^{i\alpha z} \tag{21}$$

where U_o is an initial constant vector. Upon substitution into Eq. (18), the generalized eigenvalue problem for λ, which is the vector of amplification factors, can be obtained.

$$(\hat{M} - \hat{L})v = \hat{M}\lambda v \tag{22}$$

where $\hat{M}$ and $\hat{L}$ are the Fourier symbols of M and L, respectively. The stability characteristics are determined by cycling through a fixed number of each of the spatial frequencies, in this case, 16 frequencies, in the range $0 \leqq \beta\Delta x, \gamma\Delta y, \alpha\Delta z \leqq 2\pi$ for each CFL number. The maximum eigenvalue, average eigenvalue, and the smoothing factor are determined, where the smoothing factor, defined as

$$\mu = \max\{|\lambda|\}$$
$$\text{for } \pi/2 \leqq \max(\beta\Delta x, \gamma\Delta y, \alpha\Delta z) \leqq 3\pi/2$$

and corresponds to the damping of the high frequencies and serves as an indication of how effective the multigrid procedure can accelerate convergence for a given scheme.

Results are shown in Fig. 1 for the three-factor and both of the two-factor approximate-factorization schemes. Each result was obtained by using first-order differencing on the implicit side of the equation and fully upwind, second-order differencing for the residual computations. All the calculations assume a Mach number of 0.8 and 0 deg yaw and angle of attack. Both of the two-factor schemes appear to be stable for all CFL numbers considered, whereas the three-factor scheme is only stable up to a CFL of about 20. The three-factor scheme and combination split scheme have, however, the lowest minimum smoothing factors, whereas both two-factor schemes are less sensitive to variations in the CFL number. Note that the three-factor scheme with upwind differencing is stable, whereas for central differencing, it is unstable. Since upwind schemes can be written in the form of a central difference scheme with dissipation, a stable central difference scheme should be obtainable with appropriate dissipation.

Multigrid Method

The multigrid method used in the current study is the full approximation scheme (FAS) previously implemented for central difference schemes.[7,8] For this method, a sequence of grids are introduced $G_0, G_1, \ldots, G_N$, where G_N denotes the grid points on the finest mesh and from which successively coarser grids G_i, $i = N-1, N-2, \ldots, 0$ are formed by deleting every other mesh line on the next finest grid G_{i+1}. The sequence of coarser grids is used in accelerating the convergence rate on the finest grid by efficiently reducing the low-frequency errors on the finest mesh, which can be easily shown by Fourier analysis to be the cause of slow asymptotic convergence rates.

There are several strategies for deciding when to switch from one grid level to another, generally falling under the categories of fixed or adaptive cycling algorithms. The strategies used in the present study are fixed cycling strategies including V-cycles and W-cycles. Details of these can be found in many references including Ref. 11.

Results

Three-dimensional subsonic and transonic flow computations over the ONERA M6 wing are shown below. Comparisons are made with experimental data at a Reynolds number of 11.7×10^6.[12] The wing consists of symmetrical airfoil sections with a planform swept 30 deg along the leading edge, an aspect ratio of 3.8, and a taper ratio of 0.56. Solutions are obtained for two mesh types, C-H and C-O, both of which are C-type mesh topologies around the airfoil profile. The C-H mesh has uniform spacing in the spanwise direction, whereas the C-O mesh wraps around the wingtip, consequently leading to a more precise definition of the actual rounded-tip geometry tested in the experiment. The C-O mesh has been generated with a transfinite interpolation procedure developed by Bruce Wedan of NASA Langley Research Center. The C-H mesh was obtained by simply stacking a series of two-dimensional cross sections along the span.

The first computation is the ONERA M6 wing at transonic conditions: Mach number of 0.84 and an angle of attack of 3.06 deg. Figure 2 shows the effect of multigrid on the residual and lift history for a $193 \times 33 \times 33$ C-H mesh, corresponding to 193 points along the airfoil and wake, 33 points approximately normal to the airfoil, and 33 points in the spanwise direction, 17 of which are on the wing planform. For this case, a V-cycle and four grid levels are used (a fine grid and three coarser ones). The multigrid scheme is very effective in accelerating convergence of both the residual and the lift. The residual is reduced to machine zero in 400 cycles, whereas the single grid scheme has only reduced the residual between one and two orders of magnitude. The benefit of multigrid is especially pronounced in the lift history where the final lift value is obtained to within 0.1% of its final value in 41 cycles. This is a dramatic improvement over the single grid result that required more than 400 iterations to settle in on a final lift coefficient. It should be noted that for all the cases considered, several cycles (usually five) were run with first-order spatial differencing before switching to second order.

A comparison of convergence rates between the three schemes discussed earlier is shown in Fig. 3 for identical conditions as given above, with the exception that only every other point from the $193 \times 33 \times 33$ mesh is used, resulting in a $97 \times 17 \times 17$ C-H mesh. For this size mesh, only two coarser grids are used. The three-factor, spatially split algorithm demonstrates a higher rate of convergence than either of the two-factor schemes yielding a spectral radius (that indicates the reduction in error per cycle) of approximately 0.898. The two-factor scheme in which the implicit operator is split according to the sign of the eigenvalues displays the slowest convergence rate with a spectral radius of 0.93. It should be pointed out, however, that even though the spectral radius using this scheme is not as good as for the spatially split scheme, this still represents a good improvement over a corresponding single-grid spectral radius of 0.98. All the runs on the $97 \times 17 \times 17$ meshes were made at a CFL number of 7. This was determined experimentally to be about optimum and agrees well with the CFL number for best smoothing predicted by the stability analysis. In 64-bit precision, the computational rate on the VPS-32 at NASA Langley using a V-cycle and three grid levels for the three-factor scheme is about 75 μs per grid point per cycle, whereas the two-factor eigenvalue split and combination split schemes exhibit computational rates of 140 and 85 μs per grid point per cycle, respectively. Because of the higher performance of the three-factor spatially split algorithm in both the convergence rate and the computational rate, it is used exclusively in the results that follow.

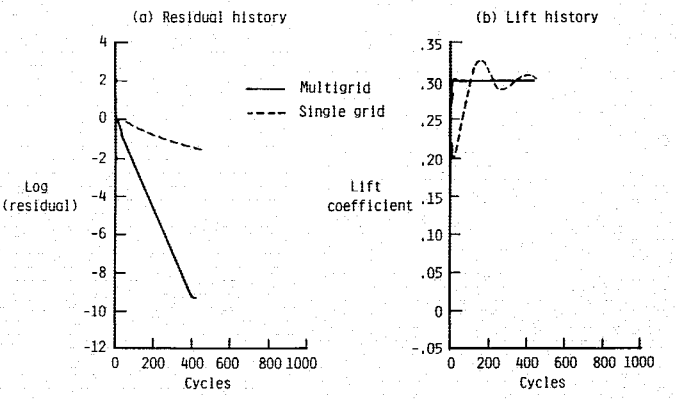

Fig. 2 Effect of multigrid on convergence, ONERA M6, $193 \times 33 \times 33$ C-H mesh, $M_\infty = 0.84$, $\alpha = 3.06$ deg.

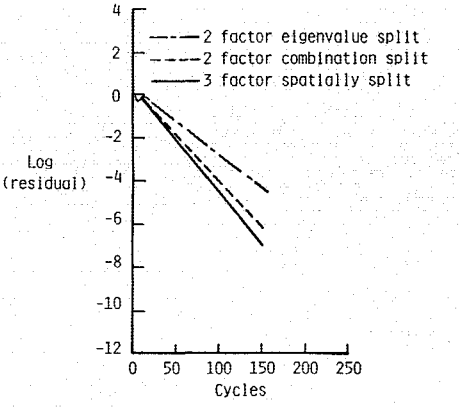

Fig. 3 Comparison of convergence rate for the three schemes, ONERA M6 wing, $97 \times 17 \times 17$ C-H mesh, $M_\infty = 0.84$, $\alpha = 3.06$ deg.

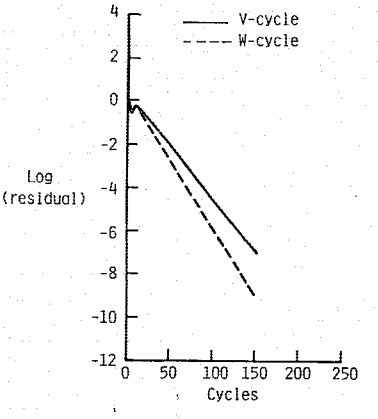

Fig. 4 Comparison of convergence rate for a V-cycle and a W-cycle, ONERA M6 wing, $97 \times 17 \times 17$ C-H mesh, $M_\infty = 0.84$, $\alpha = 3.06$ deg.

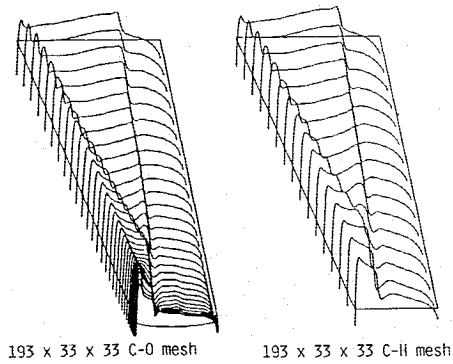

Fig. 5 Upper surface variation of pressure coefficient, ONERA M6 wing, $M_\infty = 0.84$, $\alpha = 3.06$ deg.

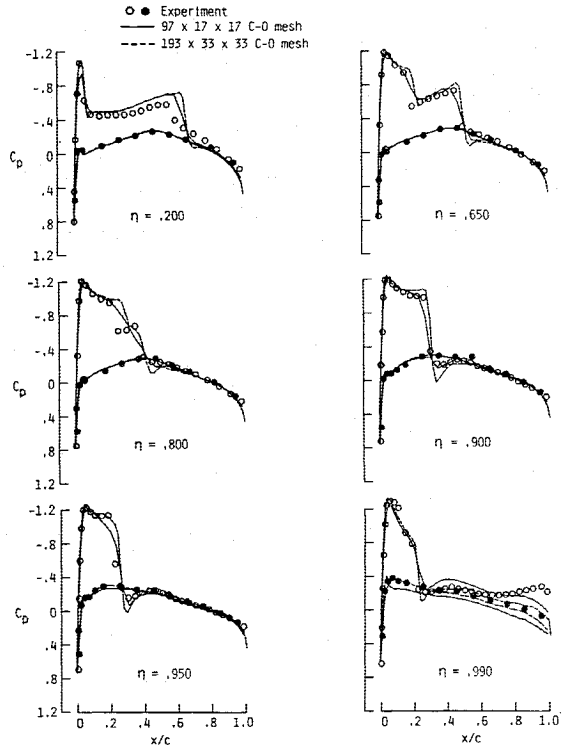

Fig. 6 Comparison of experiment and inviscid calculations using Van Leer splittings, ONERA M6 wing, $M_\infty = 0.84$, $\alpha = 3.06$ deg.

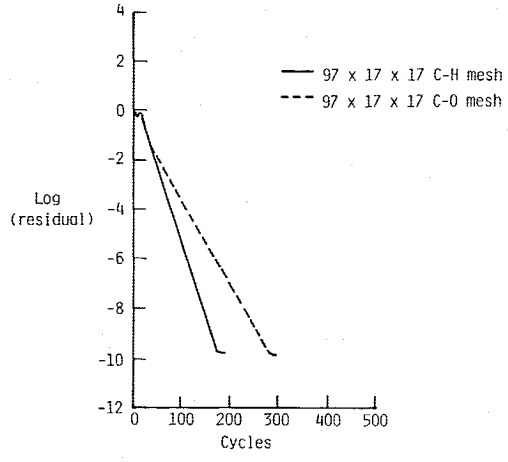

Fig. 7 Multigrid convergence for C-H and C-O meshes, ONERA M6 wing, $M_\infty = 0.699$, $\alpha = 3.06$ deg, V-cycle.

The effect of using a W-cycle over the previously used V-cycle on the residual is shown in Fig. 4 for the $97 \times 17 \times 17$ C-H mesh. An improvement using a W-cycle in the convergence rate is apparent. In addition, the lift coefficient is obtained to within 0.3% of its final value in only 14 cycles and to under 0.1% in 24 cycles. This is an improvement over the V-cycle that took 37 cycles to get the error in lift below 0.1%. Although the work involved for a W-cycle is more than for the V-cycle due to the extra smoothing iterations on the coarser grids, the time required per cycle only increased by about 13% over a V-cycle. Therefore, even though more work is involved for each cycle, a net gain is still achieved by employing the W-cycle. A summary of results for this case is given in Table 1 for $193 \times 33 \times 33$ and $97 \times 17 \times 17$ for both C-H and C-O-type grids. The table includes the spectral radius based on cycles and the number of cycles required to obtain the lift coefficient to within 0.3 and 0.1% of its final value as well as how many cycles were required to obtain the lift to five significant digits. Note that the number of cycles required for the W-cycle to obtain the lift coefficient is relatively insensitive to the number of grid points.

Figure 5 shows the upper surface pressure distributions on the $193 \times 33 \times 33$ C-H mesh as well as the $193 \times 33 \times 33$ C-O mesh. The wing under these conditions exhibits both a swept shock emanating from the apex and a nearly normal shock emanating from the root, which coalesce at about 80% of the span to form a single shock.

In Fig. 6, pressure coefficients obtained on both the $97 \times 17 \times 17$ and $193 \times 33 \times 33$ C-O meshes are compared with experimental data at six spanwise locations. The computations are obtained at the same spanwise locations as the experimental data by linear interpolation. The computations on both meshes agree reasonably well with experiment for each spanwise location; the effect of the finer mesh is that the shock is spread over a smaller spatial distance due to the smaller mesh width in the finer grid.

The next three-dimensional test case is the ONERA M6 wing at a freestream Mach number of 0.699 and an angle of attack of 3.06 deg. At these conditions, the flow remains subsonic over the entire wing. Results were obtained for this case on a $97 \times 17 \times 17$ C-O mesh, a $97 \times 17 \times 17$ C-H mesh, and both a $193 \times 33 \times 33$ C-H mesh and C-O mesh. Figure 7 shows the residual history for both the $97 \times 17 \times 17$ C-O and C-H meshes and a V-cycle. The convergence rate on the C-H mesh is slightly better than on the C-O mesh. Machine zero is reached for the C-H mesh in approximately 200 cycles, whereas the C-O mesh requires about 300 cycles, corresponding to an asymptotic spectral radius of 0.891 and 0.926, respectively. For both meshes, the lift was obtained to less than 0.1% of its final value

Table 1 Summary of results for ONERA M6 wing $M_\infty = 0.84$; $\alpha = 3.06$ deg

Mesh size and type of cycle	Cycles required to obtain C_ℓ to 0.3% of final value	C_ℓ to 0.1% of final value	C_ℓ to 5 decimal places	Spectral radius
$97 \times 17 \times 17$ C-H				
V-cycle	20	37	75	0.898
W-cycle	14	24	42	0.871
$97 \times 17 \times 17$ C-O				
V-cycle	34	45	91	0.912
W-cycle	15	27	44	0.879
$193 \times 33 \times 33$ C-H				
V-cycle	37	41	153	0.948
W-cycle	12	23	47	0.923
$193 \times 33 \times 33$ C-O				
V-cycle	27	68	149	0.952
W-cycle	14	19	47	0.926

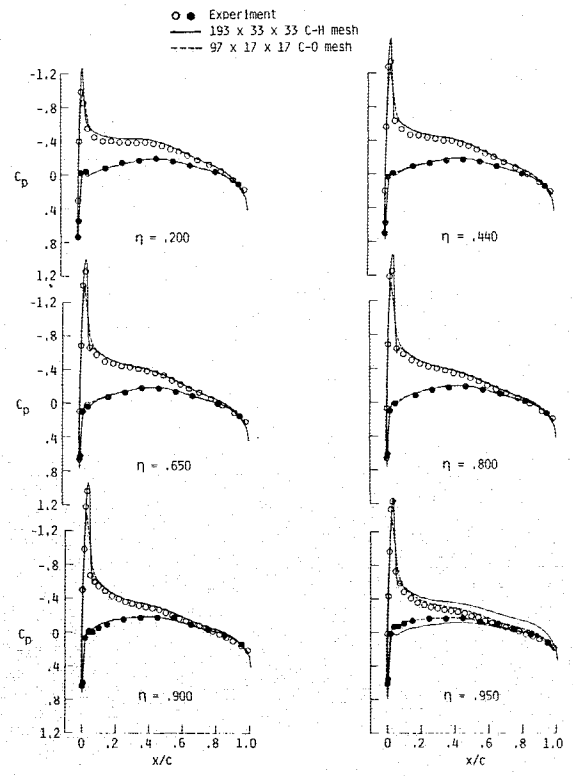

Fig. 8 Comparison of experiment and inviscid calculations using Van Leer splittings, ONERA M6 wing, $M_\infty = 0.699$, $\alpha = 3.06$ deg.

Table 2 Summary of results for ONERA M6 wing $M_\infty = 0.699$; $\alpha = 3.06$ deg

Mesh size and type of cycle	Cycles required to obtain C_t to 0.3% of final value	C_t to 0.1% of final value	C_t to 5 decimal places	Spectral radius
97 × 17 × 17 C-H				
V-cycle	19	28	38	0.891
W-cycle	11	19	33	0.866
97 × 17 × 17 C-O				
V-cycle	21	22	48	0.926
W-cycle	13	15	31	0.891
193 × 33 × 33 C-H				
V-cycle	29	37	71	0.929
W-cycle	11	21	37	0.891
193 × 33 × 33 C-O				
V-cycle	21	38	55	0.950
W-cycle	11	15	36	0.912

in less than 28 cycles, requiring only about 46 s of computer time. On the 193 × 33 × 33 C-H mesh, a spectral radius of 0.929 was obtained and a spectral radius of 0.95 was obtained on the same size C-O mesh. When using a W-cycle, a spectral radius of 0.866 is obtained for the 97 × 17 × 17 C-H mesh and one of 0.891 is obtained for the C-O mesh. Using the 193 × 33 × 33 mesh, the spectral radius using the W-cycle is also about 0.89 for the C-H mesh and 0.912 for the C-O mesh. A summary of results is given in Table 2 similar to those shown in Table 1.

The pressure distributions on the 97 × 17 × 17 C-O mesh and the 193 × 33 × 33 C-H mesh are compared with experiment at six spanwise stations in Fig. 8. At the inboard stations, the results for both meshes are essentially identical and compare well with experiment. At the outboard station, however, the pressures computed on the C-O mesh agree much closer to experiment due to the increased resolution at the tip.

Concluding Remarks

Multigrid acceleration has been applied to the three-dimensional flux-split Euler equations in generalized coordinates. Three implicit schemes have been used to smooth the errors at each grid level. Results from a linearized stability analysis of the coupled equations for each of the schemes agree well in overall trends with the numerical experiments, and indicate that the three-factor spatially split algorithm is conditionally stable (up to a CFL of about 20) but offers a slightly better smoothing rate than the other two schemes and, hence, the best multigrid performance. The stability analysis also indicates that the other two schemes, both two-factor schemes, are less sensitive to CFL variations. Results obtained for transonic and subsonic flow over the ONERA M6 wing compare well with experimental data.

Results demonstrate a substantial improvement in convergence rate using the multigrid algorithm in comparison to the single-grid algorithm. Using a W-cycle, solutions can be obtained in as few as 19 cycles for transonic conditions on a 193 × 33 × 33 mesh, whereas a V-cycle takes about 41 cycles to reach the same level of accuracy (final lift coefficient to within 0.1%). Using a V-cycle, a spectral radius of 0.891 and 0.898 is obtained for a 97 × 17 × 17 wing solution at subsonic and transonic conditions. A W-cycle for the same cases results in spectra radii of 0.866 for the subsonic case and 0.871 for the transonic case. In addition, the W-cycle is less sensitive to the size of the grid than the V-cycle for obtaining the final lift coefficient. Both of these save an order of magnitude in computing time over a single grid.

Acknowledgment

The authors acknowledge the contributions of Bruce Wedan of the Computational Fluid Dynamics Laboratory at NASA Langley Research Center, who generated the C-O mesh for the Onera M6 wing.

References

[1]Steger, J. L. and Warming, R. F., "Flux Vector Splitting of the Inviscid Gasdynamic Equation with Application to Finite Difference Methods." *Journal of Computational Physics*, Vol. 40, April 1981, pp. 263–293.

[2]Steger, J. L., "Preliminary Study of Relaxation Methods for the Inviscid Conservative Gasdynamics Equations Using Flux Splitting," NASA CR-3415, 1981.

[3]Buning, P. G. and Steger, J. L., "Solution of the Two Dimensional Euler Equations with Generalized Coordinate Transformation Using Flux-Vector Splitting," AIAA Paper 82-0971, June 1982.

[4]Van Leer, B., "Flux-Vector Splitting for the Euler Equations," Institute for Computer Applications in Science and Engineering, Rept. No. 82-30, Sept. 1982; also, *Lecture Notes in Physics*, Vol. 170, 1982, pp. 501–12.

[5]Anderson, W. K., Thomas, J. L., and Van Leer, B., "A Comparison of Finite Volume Flux Vector Splittings for the Euler Equations," AIAA Paper 85-0122, 1985.

[6]Stuben, K. and Trottenberg, U., "Multigrid Methods: Fundamental Algorithms, Model Problem Analysis and Applications," *Multigrid Methods*, Lecture Notes in Mathematics 960, Springer-Verlag, New York, Nov. 1981.

[7]Jameson, A. and Baker, T. J., "Multigrid Solution of the Euler Equations for Aircraft Configurations," AIAA Paper 84-0093, Jan. 1984.

[8]Jameson, A. and Yoon, S., "Multigrid Solution of the Euler Equations Using Implicit Schemes," AIAA Paper 85-0293, Jan. 1985.

[9]Ni, R.-H., "A Multiple-Grid Scheme for Solving the Euler Equations," *AIAA Journal*, Vol. 20, Nov. 1982, pp. 1565–1571.

[10]Beam, R. and Warming, R. F., "An Implicit Finite-Difference Algorithm for Hyperbolic Systems in Conservation-Law-Form," *Journal of Computational Physics*, Vol. 22, Sept. 1976, pp. 87–110.

[11]Anderson, W. K., "Implicit Multigrid Algorithms for the Three Dimensional Flux Split Euler Equations," Ph.D. Dissertation, Mississippi State Univ., Mississippi State, MS, Aug. 1986.

[12]Schmitt, V. and Charpin, F. "Pressure Distribution on the ONERA M6-Wing at Transonic Mach Number," AGARD Advisory Rept. 138, May 1879.